

The structures responsible for the inverse energy and the forward enstrophy cascades in two-dimensional turbulence

C.-H. BRUNEAU¹, P. FISCHER¹ and H. KELLAY²

¹ *MAB, Université Bordeaux 1, CNRS UMR 5466, INRIA projet MC2 - 351 cours de la Libération, 33405 Talence, France*

² *CPMOH, Université Bordeaux 1, CNRS UMR 5798 - 351 cours de la Libération, 33405 Talence, France*

received 25 January 2007; accepted in final form 27 March 2007

published online 27 April 2007

PACS 47.27.Ak – Fundamentals

PACS 47.27.Gs – Isotropic turbulence; homogeneous turbulence

Abstract – Two-dimensional turbulence admits two different ranges: an inverse energy cascade at large scales and a cascade of enstrophy to the small scales. Here we show that two flow structures govern the transfers of either enstrophy or energy. Vortical structures are responsible for the transfers of energy upscale while filamentary structures are responsible for the forward transfer of the enstrophy.

Copyright © EPLA, 2007

While three-dimensional turbulence is governed by a direct cascade of energy from the scale of injection to the small scales where the energy is dissipated, two-dimensional turbulence admits two different ranges [1,2]. The first one is governed by an inverse energy cascade from the scale of injection to the large scales. The second one is governed by a cascade of enstrophy from the scale of injection to the small scales. This scenario, proposed by Kraichnan and Batchelor over 40 years ago, finds confirmation in different numerical simulations and experimental realizations. However, if the scaling laws for the different ranges have been found, the links between the presence of structures and the transfer of energy or enstrophy have not been completely identified. Very recent work points out that the mechanism behind these two cascades is related to the thinning of vortices, a dominant structure in two-dimensional turbulence [3,4].

Two-dimensional turbulence has interested and continues to interest different scientific communities. Its relevance to atmospheric and oceanic flows at large scales has largely motivated its detailed study [5–7]. Its importance for the understanding of turbulence in general due to the existence of two cascades, as opposed to the direct cascade of energy in three-dimensional turbulence, is another reason to study this phenomenon. In the last decade, several experiments have been carried out to test the ideas of Kraichnan [1] and Batchelor [2] about 2D turbulence. Numerical simulations have, for much longer, identified several features of 2D turbulent flows. Now, it appears that two cascades exist in a two-dimensional turbulent flow. An

inverse energy cascade, presumably due to the merging of like sign vortices, transfers energy from the injection scale to the large scales. At scales smaller than this injection scale, an enstrophy cascade, whose origin is apparently the straining of vorticity gradients, transfers enstrophy from the large to the small scales. However, whereas the role of vortices has been identified as crucial for 2D flows [8], there has been only a few studies of the role of flow structures on the transfers of either energy or enstrophy. This is precisely what we study here. Two-dimensional turbulence admits two distinct structures: vortical structures and filamentary structures. The first are responsible for the inverse transfers of energy while the second are responsible for the forward transfer of enstrophy.

Our direct numerical simulations are motivated by experiments carried out with soap films where grid turbulence was studied in detail [9–12]. The flow studied here is obtained in a two-dimensional channel with a length of either four or five times its width and where the turbulence is generated by arrays of cylinders just like in the experiments. There are three arrays of cylinders in the flow: a first array composed of 10 cylinders placed one channel width down from the entrance produces grid turbulence while two arrays placed near the side walls of the channel and composed of 9 cylinders each reinforce the injection scale and inject even more vorticity into the flow. This configuration has been studied recently and the main results concerning the energy spectra have been reported [13]. This flow admits two ranges: an inverse cascade range and a direct enstrophy cascade range.

A similar flow configuration was studied experimentally by Rutgers showing the existence of the two cascades simultaneously [10]. In order to keep a Cartesian mesh, on which accurate finite difference schemes are written [14], the solid obstacles are considered as a porous medium of very weak permeability. So, instead of the classical Navier-Stokes equations, the following penalized Navier-Stokes equations [15,16] are solved:

$$\begin{aligned} \partial_t U + (U \cdot \nabla) U - \frac{1}{Re} \Delta U + \frac{U}{K} + \nabla p &= 0, \\ \operatorname{div} U &= 0. \end{aligned}$$

Here, $U = (u, v)$ is the velocity vector (u is the longitudinal and v is the transverse velocity), p is the pressure, Re is the nondimensional Reynolds number based on the unit inlet flow rate and length (which is 10^6 in the simulations discussed below), and K is the nondimensional coefficient of permeability of the medium. The fluid and the solid media correspond to an “infinite” and a “zero” permeability coefficient, respectively: $K = 10^{16}$ and $K = 10^{-8}$ are the values used in the numerical simulation. The above equations are associated to no-slip boundary conditions on the walls of the channel, Poiseuille flow on the entrance section and a non-reflecting boundary condition on the exit section [17]. The flow has been computed on a sequence of uniform Cartesian grids but all the results discussed in this paper have been obtained on a 2560×640 fine grid.

A typical snapshot of such a simulation is presented in fig. 1a. The cylinders are apparent both near the side walls and at one distance down from the entrance. The vorticity field of this flow produced at a Reynolds number of 50000 (calculated using the diameter of the cylinders which is 0.05 in units of channel width), is shown in fig. 1a. The role of the side cylinders is crucial in producing an inverse cascade range as has been shown by Rutgers [10] and Bruneau and Kellay [13]. This is the flow field we analyze here using techniques based on wavelet analysis. Contrary to standard Fourier analysis, the wavelet decomposition we use here reveals the different structures of the flow at all spatial scales. This is also different from other filtering techniques where averaging over a certain range of scales is carried out.

The theory of wavelet packets has been developed more than ten years ago [18]. The wavelet analysis is based on a decomposition on a basis, like Fourier analysis, but with basis functions localized in physical and Fourier spaces. A sketch of the theory with application to 2D turbulence analysis and filtering is given in [19] where a few tests are performed in order to get the best wavelet mother and to determine how many levels are necessary to get an efficient representation of the flow. A complete decomposition from a $2^n \times 2^n$ fine grid requires n levels to reach the coarsest level corresponding to the mean flow. Here, it is necessary to perform the wavelet packets decomposition at least on five levels to

get a good representation of the large-scale structures. Daubechies-type wavelets are used in the current paper to build the packets array, and the entropy criterion is used in the best basis selection process. Once the velocity components are decomposed on such a basis, they are split into two orthogonal subfields using a threshold on the wavelet packets coefficients giving one subfield for the strong coefficients and another for the weaker ones. These subfields are therefore not determined by using a threshold value on the modulus of the velocity or vorticity as in [20] but by their representation on the basis. The two subfields are continuous and can occupy the same physical space contrary to a decomposition based on thresholding the modulus directly which introduces artificial discontinuities in the filtered field. For a particular choice of the threshold, the vorticity field reconstructed from these subfields is dominated by two types of structure. For the strong coefficients, greater than the fixed threshold, vortical structures, with what seems to be the solid rotation part of the vortices, are obtained as seen in fig. 1b. For the small coefficients, filamentary structures are obtained as seen in fig. 1c. A zoom on a filamentary structure is shown in fig. 1d and shows that these filaments have a spiral shape. By opposition to a Fourier-based filtering, the present orthogonal filtering already used in [21] does not separate the scales of the flow but the type of structures. Here the two subfields are not seen like vortical coherent structures and background as was supposed in previous studies, but like two coherent and multiscale subfields with their own dynamics. We refer to the two subfields as the vortical structures and the filamentary structures. The vortical structures carry some 95% of the energy and 70% of the total enstrophy. The filaments on the other hand carry only 5% of the energy but 30% of the enstrophy. The energy and enstrophy content of each subfield is very different.

Thus, the filtering based on this wavelet decomposition reveals two different structures: vortical structures and filamentary structures which encompass both the regions occupied by the vortices and the regions between vortices. The filaments have a clear spiral shape in the regions occupied by the vortices. The question we ask here is what is the role of these structures in the establishment of the energy or enstrophy transfers present in two-dimensional turbulence. In order to answer this question we study the energy flux and the enstrophy flux associated with each subfield.

We focus on two invariants of two-dimensional turbulence namely the energy $E \equiv \langle \frac{1}{2} |U|^2 \rangle$ and the enstrophy $Z \equiv \langle \frac{1}{2} |\omega|^2 \rangle$, where ω is the scalar vorticity. The energy balance in Fourier space is obtained by applying a Fourier transform to the corresponding energy balance in physical space with the result

$$\partial_t E(\mathbf{k}) = T_E(\mathbf{k}) + D(\mathbf{k})E(\mathbf{k}) + F(\mathbf{k}),$$

where $\mathbf{k} = (k_x, k_y)$ is the Fourier variable (the wave vector) in Fourier space, E the energy density, T_E the nonlinear

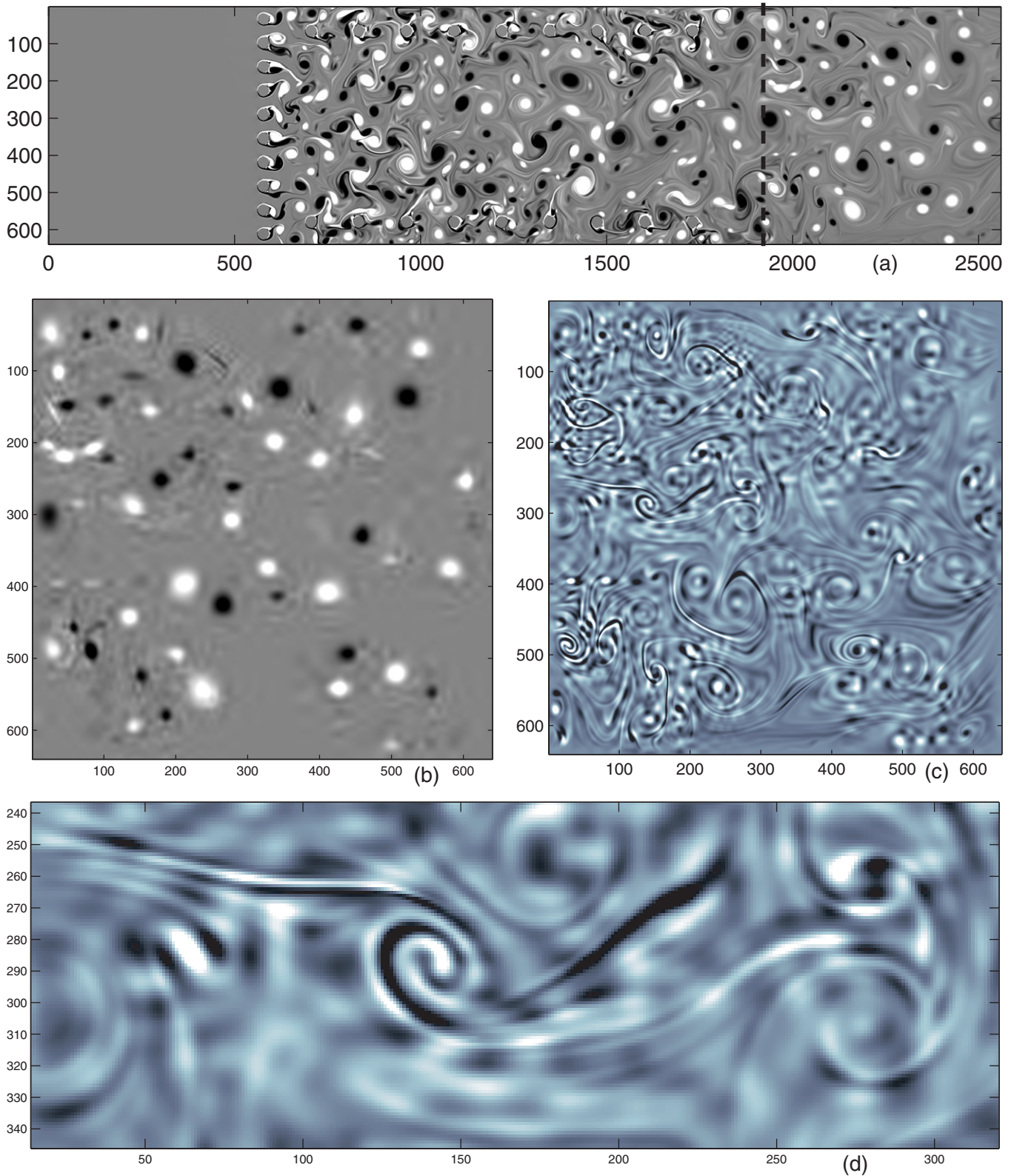


Fig. 1: a) Snapshot of the vorticity field for the whole flow. b) Vortical structures corresponding to the high coefficients from the wavelet analysis. c) Filamentary structures corresponding to the small coefficients from the wavelet analysis. d) A zoom on a filamentary structure.

energy transfer, D the dissipation operator and F stands for the energy injection. In our experiments, there is no artificial injection since the turbulence is naturally generated by the obstacles, so $F = 0$. To study the energy

transfer we focus on the nonlinear energy transfer function which, due to the orthogonal decomposition, can be written as

$$\begin{aligned} T_E(\mathbf{k}) &= \widehat{U}^*(\mathbf{k}) \cdot (U \cdot \widehat{\nabla}) U(\mathbf{k}) \\ &= \widehat{U}_s^*(\mathbf{k}) \cdot (U \cdot \widehat{\nabla}) U_s(\mathbf{k}) + \widehat{U}_s^*(\mathbf{k}) \cdot (U \cdot \widehat{\nabla}) U_f(\mathbf{k}) \\ &\quad + \widehat{U}_f^*(\mathbf{k}) \cdot (U \cdot \widehat{\nabla}) U_s(\mathbf{k}) + \widehat{U}_f^*(\mathbf{k}) \cdot (U \cdot \widehat{\nabla}) U_f(\mathbf{k}), \end{aligned}$$

where the subscript s stands for the subfield dominated by vortical structures and the subscript f stands for the vorticity filaments subfield ($U = U_s + U_f$). The velocities U_s and U_f are the result of the orthogonal decomposition of the velocity vector field through the use of the wavelet filtering discussed above. The global energy transfer can be split into four parts corresponding to the multiscale transfers for each subfield or from the interaction between the two subfields. For instance, $\widehat{U}_s^*(\mathbf{k}) \cdot (U \cdot \widehat{\nabla}) U_f(\mathbf{k})$ is the energy transfer from the interaction between the vorticity filaments subfield and the solid rotation subfield. Here we did not split the advection operator $U \cdot \nabla$ into its two components for simplicity but it should be noted here that the $U_s \cdot \nabla$ plays the major role. An integration over the angle is then carried out to obtain the transfers *vs.* the wavenumber k (the modulus of \mathbf{k}). The fluxes $\Pi_E(k)$ are computed as $\int_k^{k_{\max}} T_E(k') dk'$. The fluxes corresponding to each term in the expression for the total transfer function will be denoted as, for example, $\Pi_E^{f \rightarrow s}$ which is the flux corresponding to the transfer term above. In the same way the nonlinear enstrophy transfer term $T_Z(\mathbf{k}) = \widehat{\omega}^*(\mathbf{k}) (U \cdot \widehat{\nabla}) \omega(\mathbf{k})$ is split into four parts using $\omega = \omega_s + \omega_f$ and the enstrophy fluxes Π_Z are computed.

The most important aspect of our study is that the fluxes associated with each structure as well as the fluxes associated with the interactions of the two structures can be obtained separately. The total energy and enstrophy fluxes are displayed in fig. 2. $\Pi_E(k)$ shows the typical behavior associated with the existence of two cascades. At large scales (small k), the energy flux is negative indicating an inverse transfer of energy, *i.e.* from the injection scale to the large scales. In addition to this, the flux becomes zero at the injection scale. The injection scale here is close to the size of the cylinders (corresponding to a wavenumber $k = 20$). *A priori* and if the turbulence is inertial, the energy flux should present a plateau in the small wavenumber range. Our simulations do not produce this plateau and the most probable reason for this is the limitation of the range of scales probed and the presence of the boundary.

The enstrophy flux displayed in fig. 2b is on the other hand positive for scales smaller than the injection scale (or high wavenumber k) indicating a forward enstrophy cascade to the small scale end. The enstrophy flux then becomes zero and turns negative at the low-wavenumber end or large scales. The zero crossing corresponds to the injection scale. Both the energy flux and the enstrophy flux show that the classical picture of 2D turbulence,

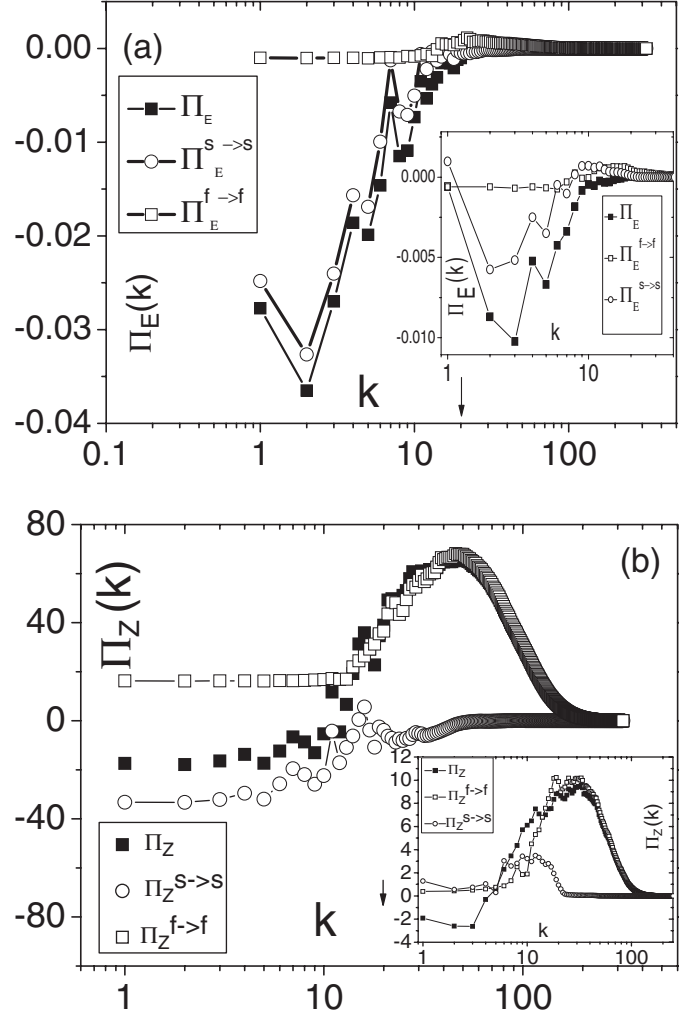


Fig. 2: Turbulence produced by arrays of cylinders: a) Energy flux for the full field and the filtered fields. b) Enstrophy flux for the whole field and for the filtered fields. The arrow corresponds to $k_{\text{injection}}$. Insets: turbulence produced by arrays of vortices: a) Energy flux for the full field and the filtered fields. b) Enstrophy flux for the whole field and for the filtered fields.

i.e. coexistence of two cascades, is valid for the flow considered here regardless of whether a plateau for the energy flux or enstrophy flux is achieved.

Now let us examine the consequences of the decomposition which reveals the existence of two distinct structures. Let us first consider the energy and enstrophy fluxes associated with the vortical structures. This is the flux associated with the first term in the expression for the energy transfer function and noted $\Pi_E^{s \rightarrow s}$. The corresponding enstrophy flux is denoted $\Pi_Z^{s \rightarrow s}$. The energy flux for these structures shows a large negative part at small k , which is similar to the total flux, and becomes very small and close to zero beyond the injection scale. The enstrophy flux on the other hand is negative at small k and becomes close to zero beyond the injection scale. The fluxes associated with the filaments and denoted $\Pi_E^{f \rightarrow f}$ and $\Pi_Z^{f \rightarrow f}$ for the energy and the enstrophy flux, respectively, are also

displayed in figs. 2a and b. The energy flux associated with the filaments is negative but small at small k and becomes slightly positive near the injection scale before becoming zero at the high- k end. The enstrophy flux for the filaments is on the other hand large and positive for the high- k end (smaller than the injection scale) and is very close to the value of the total flux in this region of wavenumber. The examination of these fluxes indicates that the main part of the energy flux comes from the subfield dominated by vortical structures while the main part of the enstrophy flux comes from the subfield dominated by filamentary structures. This is the main finding of our study: We identify two distinct structures which are responsible for the transfers of energy upscale (the vortical structures) and the enstrophy transfer downscale (the filamentary structures). This finding is robust with respect to the spatial resolution of the simulations as other runs with higher spatial resolution (4096×1024) and smaller Reynolds number (5000) give similar results. To our knowledge, this is a new illustration of the role of flow structures in turbulence and shows the power of wavelet filtering in the understanding of complex flows by revealing some of their properties in physical space.

The properties of the turbulent cascades in two-dimensional turbulence have been examined previously in physical space for the passive scalar field as well as the vorticity field. These studies are based on the orientation dynamics of tracer gradients and of vorticity gradients and use refined diagnostic techniques to partition the flow into different regions [22,23]. While the strain-dominated regions turn out to be the most active for the enstrophy cascade, rotation-dominated regions can also contribute to the growth of vorticity gradients [24–26]. These studies point out that the physical space picture of the transfers brings in additional information about the properties of turbulence. A more recent analysis of a two-dimensional turbulent field through a spatial filtering technique [3] allowed to show that the enstrophy is cascading downscale and that the spatial regions where this occurs are dominated by strain. These results have also been obtained in an experiment with soap films [11]. Our results are in agreement with the conclusions of these studies and point out that the filaments are fully responsible for the transfers of enstrophy downscale. They refine and reconcile previous studies in the sense that it is not just the strain regions that are active in the transfers of enstrophy but the regions dominated by the presence of filaments which occur principally in the strain regions but extend to regions where the vortical structures exist as well. Our study also clarifies unambiguously the role of the vortices in the transfer of energy upscale. A study of the spatial structure of energy transfers in 2D turbulence by Babiano and Dubos [27] also concluded that the strongly energetic active regions are localized around coherent vortices. More recently, a mechanism where the thinning of vortices turns out to play a major role for the upscale energy transfer was proposed [4]. While fig. 1b

does show the presence of elongated vortices, it is rather difficult at present to make a direct link between our findings and the proposed mechanism.

A natural extension of our analysis is a study of the alignments between vorticity gradients and the direction of stretching for the filament field since, and as suggested by Protas, Babiano and Kevlahan [28], the filaments tend to be aligned with the stretching direction giving rise to the transfer of enstrophy downscale. This alignment property was studied for different scales in the enstrophy cascade range and found to hold in the strain regions for sufficiently small scales [3]. In addition, and since our analysis is capable of isolating the structures involved in the upscale transfer of energy, a local study of the dynamics of vortex thinning and its influence on the surrounding large-scale field would be very instructive and may allow to probe the proposed mechanism for the inverse cascade in detail. Such physical space analysis should also allow a refined study of the inverse cascade to determine whether it is vortex mergers or the formation of large clusters of like sign vortices, as suggested by experiments [29], which dominate the flow structure.

One may ask whether the presence of the cylinders is the main agent for producing the filamentary structures. We have tested this by simulating a turbulent flow in a channel with a length of five times its width where about 500 vortices (size $1/10$ or $1/20$ of the channel width and therefore comparable to the injection scale for the cylinder case) were placed randomly in the channel. The evolution of this ensemble was then analyzed in a similar way as for the cylinder case. Vortical structures and filaments, which develop after a few turnover times and produced by the interactions between the vortices, were obtained. The wavelet filtering and the calculated fluxes give similar results as for the cylinder case. These fluxes are shown in the insets of figs. 2a and b. Here the filaments are responsible for the enstrophy flux while the vortical structures are responsible for the energy flux just like for the cylinder case showing that the existence of these flow structures and their role in transferring either the energy upscale or the enstrophy downscale is inherent to 2D turbulent flows.

The wavelet analysis of a two-dimensional turbulent flow shows that the vorticity field can be decomposed into two orthogonal subfields. Each subfield is characterized by a distinct structure: vortices or filaments. While the vortical structures are responsible for the transfer of energy upscale, the filamentary structures are responsible for the transfer of enstrophy downscale. Additional work is required to understand the link between the present findings and recently proposed mechanisms for the enstrophy and energy cascades.

REFERENCES

- [1] KRAICHNAN R. H., *Phys. Fluids*, **10** (1967) 1417.
- [2] BATCHELOR G. K., *Phys. Fluids*, **12** (1969) II-233.

- [3] CHEN S., ECKE R. E., EYINK G. R., WANG X. and XIAO Z., *Phys. Rev. Lett.*, **91** (2003) 214501.
- [4] CHEN S., ECKE R. E., EYINK G. L., RIVERA M., WAN M. and XIAO Z., *Phys. Rev. Lett.*, **96** (2006) 084502.
- [5] MOREL P. and LARCHEVEQUE M., *J. Atmos. Sci.*, **31** (1974) 2189.
- [6] LINDBORG E., *J. Fluid Mech.*, **388** (1999) 259.
- [7] TUNG K. and ORLANDO W., *J. Atmos. Sci.*, **60** (2003) 824.
- [8] MCWILLIAMS J. C., *J. Fluid Mech.*, **146** (1984) 21; **219** (1990) 361.
- [9] KELLAY H., WU X. L. and GOLDBURG W. I., *Phys. Rev. Lett.*, **74** (1995) 3975.
- [10] RUTGERS M., *Phys. Rev. Lett.*, **81** (1998) 2244.
- [11] RIVERA M. K., DANIEL W. B., CHEN S. Y. and ECKE R. E., *Phys. Rev. Lett.*, **90** (2003) 104502.
- [12] KELLAY H. and GOLDBURG W. I., *Rep. Prog. Phys.*, **65** (2002) 845.
- [13] BRUNEAU C. H. and KELLAY H., *Phys. Rev. E*, **71** (2005) 046305.
- [14] BRUNEAU CH. H. and SAAD M., *Comput. Fluids*, **35** (2006) 326.
- [15] ANGOT P., BRUNEAU C. H. and FABRIE P., *Num. Math.*, **81** (1999) 497.
- [16] BRUNEAU CH. H. and MORTAZAVI I., *Int. J. Num. Methods Fluids*, **46** (2004) 415.
- [17] BRUNEAU C. H. and FABRIE P., *Int. J. Num. Methods Fluids*, **19** (1994) 693.
- [18] FARGE M., GOIRAND E., MEYER Y., PASCAL F. and WICKERHAUSER M., *Fluid Dyn. Res.*, **10** (1992) 229.
- [19] FISCHER P., *Discr. Cont. Dynam. Syst. B*, **5** (2005) 659.
- [20] BORUE V., *Phys. Rev. Lett.*, **72** (1994) 1475.
- [21] KEVLAHAN N. K.-R. and FARGE M., *J. Fluid Mech.*, **346** (49) 1997.
- [22] HUA B. L. and KLEIN P., *Physica D*, **113** (1998) 98.
- [23] LAPEYRE G., KLEIN P. and HUA B. L., *Phys. Fluids*, **11** (1999) 3729.
- [24] LAPEYRE G., HUA B. L. and KLEIN P., *Phys. Fluids*, **13** (2001) 251.
- [25] KLEIN P., HUA B. L. and LAPEYRE G., *Physica D*, **146** (1999) 246.
- [26] DUBOS T. and BABIANO A., *J. Fluid Mech.*, **492** (2003) 131.
- [27] BABIANO A. and DUBOS T., *J. Fluid Mech.*, **529** (2005) 97.
- [28] PROTAS B., BABIANO A. and KEVLAHAN N. K.-R., *Physica D*, **12** (1999) 169.
- [29] PARET J. and TABELING P., *Phys. Fluids*, **10** (1998) 3126.